University of Reading

Auroral and non-auroral H3+ ion winds at Uranus with Keck-NIRSPEC and IRTF-iSHELL

Article

Published Version

Creative Commons: Attribution 4.0 (CC-BY)

Open Access

Thomas, E. M., Stallard, T. S., Melin, H., Chowdhury, M. N., Moore, L., O'Donoghue, J. ORCID: https://orcid.org/0000-0002-4218-1191, Johnson, R. E., Wang, R., Knowles, K. L., Tiranti, P. I., Dello Russo, N., Ron J. Vervack, J. and Kawakita, H. (2025) Auroral and non-auroral H3+ ion winds at Uranus with Keck-NIRSPEC and IRTF-iSHELL. Geophysical Research Letters, 52 (7). e2024GL112001. ISSN 1944-8007 doi: 10.1029/2024GL112001 Available at https://centaur.reading.ac.uk/122205/

It is advisable to refer to the publisher's version if you intend to cite from the work. See Guidance on citing.

To link to this article DOI: http://dx.doi.org/10.1029/2024GL112001

Publisher: American Geophysical Union

All outputs in CentAUR are protected by Intellectual Property Rights law, including copyright law. Copyright and IPR is retained by the creators or other copyright holders. Terms and conditions for use of this material are defined in the End User Agreement.

University of Reading

www.reading.ac.uk/centaur

CentAUR

Central Archive at the University of Reading

Reading's research outputs online

Check for updates

Geophysical Research Letters

RESEARCH LETTER
10.1029/2024GL112001

Auroral and Non-Auroral H_3^+ Ion Winds at Uranus With Keck-NIRSPEC and IRTF-iSHELL

Emma M. Thomas[1], Tom S. Stallard[1], Henrik Melin[1], Mohammad N. Chowdhury[2], Luke Moore[3], James O'Donoghue[4], Rosie E. Johnson[5], Ruoyan Wang[2], Katie L. Knowles[1], Paola I. Tiranti[1], Neil Dello Russo[6], Ron J. Vervack Jr.[6], and Hideyo Kawakita[7]

[1]Department of Mathematics, Physics & Electrical Engineering, Northumbria University, Newcastle Upon Tyne, UK, [2]School of Physics and Astronomy, University of Leicester, Leicester, UK, [3]Center for Space Physics, Boston University, Boston, MA, USA, [4]Department of Meteorology, University of Reading, Reading, UK, [5]Department of Physics, Prifysgol Aberystwyth University, Aberystwyth, UK, [6]Johns Hopkins Applied Physics Laboratory, Laurel, MD, USA, [7]Koyama Astronomical Observatory, Kyoto Sangyo University, Kyoto, Japan

Key Points:

- The second ever detection of IR H_3^+ aurora at Uranus, potentially the first to align with Uranus's southern magnetic pole
- Ion winds are successfully detected at Uranus with an average super rotation found across multiple days, likely caused by global thermospheric processes or magnetospheric coupling
- Several locations were found to rotate 7%–20% faster than the planetary rotation, with one location aligning with the southern aurora

Supporting Information:

Supporting Information may be found in the online version of this article.

Correspondence to:

E. M. Thomas,
emma.m.thomas@northumbria.ac.uk

Citation:

Thomas, E. M., Stallard, T. S., Melin, H., Chowdhury, M. N., Moore, L., O'Donoghue, J., et al. (2025). Auroral and non-auroral H_3^+ ion winds at Uranus with Keck-NIRSPEC and IRTF-iSHELL. *Geophysical Research Letters*, *52*, e2024GL112001. https://doi.org/10.1029/2024GL112001

Received 14 NOV 2024
Accepted 6 MAR 2025

Author Contributions:

Data curation: Henrik Melin, Luke Moore, Neil Dello Russo, Ron J. Vervack Jr., Hideyo Kawakita
Formal analysis: Emma M. Thomas, Tom S. Stallard, Henrik Melin
Methodology: Emma M. Thomas, Tom S. Stallard
Software: Emma M. Thomas, Henrik Melin, Mohammad N. Chowdhury, Ruoyan Wang
Supervision: Tom S. Stallard, Henrik Melin
Validation: Tom S. Stallard
Writing – original draft: Emma M. Thomas, Tom S. Stallard, Henrik Melin

© 2025. The Author(s).
This is an open access article under the terms of the Creative Commons Attribution License, which permits use, distribution and reproduction in any medium, provided the original work is properly cited.

Abstract To date, no investigation has documented ionospheric flows at Uranus. Previous investigations of Jupiter and Saturn have demonstrated that mapping ion winds can be used to understand ionospheric currents and how these connect to magnetosphere-ionosphere coupling. We present a study of Uranus's near infrared emissions (NIR) using data from the Keck II Telescope's Near InfraRed SPECtrograph (NIRSPEC) and the InfraRed Telescope Facility's iSHELL spectrograph. H_3^+ emission lines were used to derive dawn-to-dusk intensity, ionospheric temperatures and ion densities to identify auroral emissions, with their Doppler shifts used to measure ion velocities. We confirm the presence of the southern NIR aurora in 2016, driven by elevated H_3^+ column densities up to 6.0×10^{16} m^{-2}. While no auroral emissions were detected in 2014, we find a 14%–20% super rotation across the planet's disk in 2014 and a 7%–18% super rotation in 2016.

Plain Language Summary To date, no investigation has documented the motion of ions in Uranus's upper atmosphere. Previous investigations of Jupiter and Saturn have demonstrated that mapping ion winds can highlight the motion of ionospheric currents and trace out the connections between a planet's upper atmosphere and magnetic field. We present a study of Uranus's near infrared emissions (NIR) using data from the Keck II Telescope's Near InfraRed SPECtrograph (NIRSPEC) and the InfraRed Telescope Facility's iSHELL spectrograph. H_3^+ emission lines were analyzed for intensity, temperature and ion density fluctuations to identify auroral emissions, and for the first time investigate the motion of H_3^+ at Uranus. We confirm the existence of the southern NIR aurora observed in 2016 which is driven by high H_3^+ column densities, up to 30 times stronger than prior investigations. While no auroral emissions were seen in 2014, we find a 14%–20% increase in the ion speeds compared to the rotation of the planet in 2014 and a 7%–18% increase in ion speeds observed in 2016.

1. Introduction

Auroral emissions at Uranus were first detected by the Voyager 2 spacecraft in 1986 (Herbert, 2009; Herbert & Sandel, 1994). These ultraviolet (UV) emissions revealed a unique auroral system compared to those of Earth, Jupiter and Saturn. Since then, UV observations from the Hubble Space Telescope have redetected portions of both the southern and northern aurora (Lamy, 2020; Lamy et al., 2012, 2017, 2018). At Jupiter and Saturn, UV and NIR observations have been key in identifying how the aurorae are generated and understanding its response to effects on the ionosphere and magnetosphere. The NIR northern aurora was first detected by Thomas et al. (2023) with a possible southern aurora observation by Melin et al., 2019. Both studies use H_3^+, a triatomic hydrogen ion, to identify the NIR aurora.

H_3^+ is a key tracer of energy and ion populations in Uranus's ionosphere and models suggest that the density peak sits between altitudes of 1,000 km and 3,000 km (Moore et al., 2020). Observations of H_3^+ have highlighted the characteristics of ionospheric flows at both Jupiter and Saturn (Miller et al., 2020), where ion velocities derived from Doppler shifts have enabled extensive studies of ion winds associated with both Jupiter and Saturn's aurora (Stallard et al., 2001, 2007a, 2008, 2012; Chowdhury et al., 2019, 2022; Johnson et al., 2017). For Jupiter, the auroral region consists of a broad anti-clockwise rotation across the northern main auroral region (Johnson

Writing – review & editing: Emma M. Thomas, Tom S. Stallard, Henrik Melin, Mohammad N. Chowdhury, Luke Moore, James O'Donoghue, Rosie E. Johnson, Ruoyan Wang, Katie L. Knowles, Paola I. Tiranti, Neil Dello Russo, Ron J. Vervack Jr., Hideyo Kawakita

et al., 2017; Stallard et al., 2001). This matches plasma flows within Jupiter's magnetosphere and flows in the same direct within the thermosphere but is weaker in flow at this altitude (Wang et al., 2023). This suggests that H_3^+ in Jupiter's auroral ionosphere is strongly coupled with the magnetosphere. Saturn has equally intriguing H_3^+ velocities, with the entire auroral ionosphere undergoing a similar anti-clockwise motion, matching with observed plasma flows in the magnetosphere (Stallard et al., 2004, 2007a, 2007b). Investigations have also revealed complex flow arcs at the northern pole (Stallard et al., 2019), as well as rotating ionospheric twin polar vortex, presumably driven by a matching twin vortex within the neutral atmosphere (Chowdhury et al., 2022).

Away from the auroral regions, supersonic jets have been observed at Jupiter using UV observations (Emerich et al., 1996); however no comparable H_3^+ ion velocities were observed (Johnson et al., 2017). At Saturn the weak emission from H_3^+ at equatorial regions (O'Donoghue et al., 2019) has prevented any measurement of ion wind flows at sub-auroral latitudes. However, during Cassini's Grand Finale orbits, Khurana et al. (2018) analyzed field-aligned currents at Saturn's equator inside the D ring. They showed that currents could be generated by velocity shears in the zonal winds of Saturn's upper atmosphere. The presence of these currents was consistent with zonal wind flows in the troposphere which could extend high into the thermosphere, and so we may expect similar current systems at Uranus.

For Uranus, it is difficult to predict the ionospheric flows as modeling the complex magnetic field (Ness et al., 1986) is still ongoing (Cao & Paty, 2017, 2021; Tóth et al., 2004). An initial theory by Vasyliunas (1986) suggested that corotation may not be the dominant state for the planet's magnetosphere at solstice, as the configuration of Uranus's magnetic field is at times parallel or perpendicular with the solar wind and "allow convection to penetrate deep into the inner magnetosphere." The ionospheric convection expected from either a parallel or perpendicular magnetic field has not been modeled to date. Jupiter and Saturn provide unreliable comparisons, due to the vastly different magnetic field configuration and faster rotation speeds.

Here, using high spectral resolution H_3^+ observations we conduct the first analysis of ion winds at Uranus. We use the same methods described above at Jupiter and Saturn to analyze ion velocities. We reanalyze the possible NIR auroral event from October 2016 by extracting temperature and column densities at the same location as the observed enhanced intensities. If the event is confirmed to be auroral, the ion winds may give the first insight into ionospheric flows at and around the aurora.

2. Observations and Analysis

On 13 October 2014 Uranus was observed with NIRSPEC on the NASA Keck II Telescope (McLean et al., 1998), and on 11 October 2016 using iSHELL on the NASA Infrared Telescope Facility (Rayner et al., 2012), where both telescopes are based near the summit of Maunakea, Hawai'i. In both 2014 and 2016, Uranus's equatorial diameter subtended 3.7" on the sky with a sub-Earth latitude of −27° in 2014 and −36° in 2016 as shown in Figures 1a and 1b. Tabulated in Supplementary Table S1 in Supporting Information S1, we set both the NIRSPEC and iSHELL slits parallel to the planetary equator. In 2014, the slit was stationary, whereas in 2016, the slit was moved to 3 set locations (shown in Figure 1b) to increase latitudinal coverage. For our analysis, we measured the H_3^+ ν_2 Q(1, 0$^-$) and ν_2 Q(3, 0$^-$) emission lines at 3.953 and 3.985 μm, using spectral resolutions of ∼25,000 and ∼75,000 with Keck II NIRSPEC and IRTF iSHELL respectively (spectral images shown in Figures 1c–1f).

Supplementary Table S1 in Supporting Information S1 highlights the difference in integration times for each pair where Uranus's slit position was alternated between the top half (A) and bottom half (B) of the slit. A longer exposure time was needed in 2016, due to the smaller telescope aperture of IRTF compared to Keck. For the 2014 data, after sky subtraction, we coadded72 frames into 9 coadded sets with a SNR of ∼10. To match the integration time between the 2014 and 2016 data sets, only 6 of the 9 sets of data were used from 2014 with each set integrated over an 8-min period. For the 2016 data, four sets of AB frames were coadded resulting in a total 11 sets of ABABABAB frames, each integrated over a 13-min period.

To determine the intensity, temperature and column densities of H_3^+ at Uranus, this study focused on emission lines Q(1, 0$^-$) and Q(3, 0$^-$) which were averaged for the intensity and ion velocities to increase the SNR, whereas temperature and column density measurements required these lines to be separate. The data were reduced in the same process shown in Thomas et al. (2023), Melin et al. (2019). The intensity was then calculated using the same steps as Thomas et al., 2023. The H_3^+ ro-vibrational temperatures were calculated using the Q(1,0$^-$) and Q(3, 0$^-$) emission lines, via Equations 1, 2 and 3 discussed in Johnson et al. (2018). The column density, N(H_3^+), which is

19448007, 2025, 7, Downloaded from https://agupubs.onlinelibrary.wiley.com/doi/10.1029/2024GL112001 by James O'Donoghue - Test , Wiley Online Library on [02/04/2025]. See the Terms and Conditions (https://onlinelibrary.wiley.com/terms-and-conditions) on Wiley Online Library for rules of use; OA articles are governed by the applicable Creative Commons License

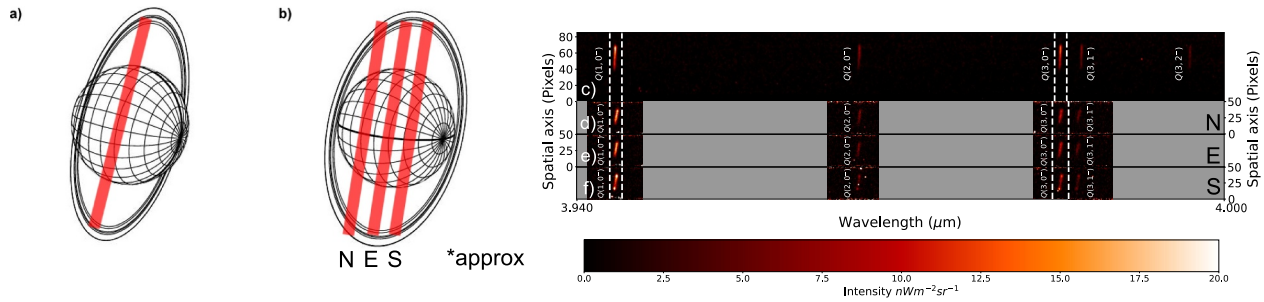

Figure 1. The geometry of Uranus as seen from Earth in panel (a) 2014 and (b) 2016. The orientation of the spectrograph slit is shown in red and overlaid. (c) The average H_3^+ spectrum for Uranus as observed by Keck II NIRSPEC between 3.95–4.0 μm. Whereas (d), (e) and (f) present the average H_3^+ emission spectrum for Uranus as observed by IRTF iSHELL between 3.95–4.0 μm with the Q(1, 0$^-$) and Q(3, 0$^-$) emission lines highlighted with dashed white lines at slit position (d) Equator (E), (e) North (N) and (f) South (S).

a measurement of the ion density in a column of the planet's atmosphere can be calculated via Equations 4 and 5 in Johnson et al. (2018). The emission from the H_3^+ is optically thin, allowing observations to view radiation from deep in the planet's upper atmosphere.

The intensities are projected onto a Uranian Longitude System (ULS) longitude and latitude map, using the same steps as Thomas et al., 2023. The exact central meridian longitude (CML) is unknown during either set of observations due to the loss of known ULS longitude since 1986 from the ±0.01 uncertainty on the planet's rotation rate, which results in a ±180° uncertainty after ~1.75 years (Ness et al., 1986). Lamy et al. (2017) relocated the southern ULS magnetic pole in November 2014 (104 ± 26°), which we can use to predict the CML in the ULS longitude system for the 13 October 2014 observations (~211 ± 30° CML); however, we cannot do the same for the 2016.

To detect the H_3^+ ion winds, we use Equation 8 from Johnson et al. (2017) to convert the Doppler shift into a measured line of sight (LOS) velocity (v_m). The change in wavelength per pixel ($\Delta\lambda$) was calculated as 6.118×10^{-5} μm (using skylines) for Keck II NIRSPEC and 1.570×10^{-5} μm for IRTF iSHELL. The resulting velocity is the relative ion wind velocity in the observer's reference frame (v_{ORF}) and should be compared against the planetary rotation (v_r) to highlight any super or sub rotation in the ionospheric velocities. For this investigation, we assumed that H_3^+ predominantly sits at 3,000 km above the planet's surface (Moore et al., 2019). We include the effects of sub-Earth latitude in our calculation of v_r across Uranus. Away from Uranus's equinox in 2007, the sub-Earth latitude angle (SEL) continues to increase which decreases the magnitudes of v_{ORF} and v_r, since the scalar product between the rotational velocity vector and the LOS vector becomes smaller, the resulting change is shown in Equation 1 and Equation 2.

$$v_{r0} = \left(\frac{R_{H3+} \times 2 \times \pi}{\tau \times 60 \times 60}\right) \quad (1)$$

$$v_r = \left(\frac{y'}{R_{\text{Pixels}}}\right) \times (v_{r0}) \times \sin(90 - \text{SEL}) \quad (2)$$

where v_{r0} is the LOS velocity at the equatorial limb, R_{H3+} is the radial altitude where the H_3^+ sits at in km, τ is the planetary rotation rate in hr, y' is the distance in pixels from the center of the planet, R_{Pixels} is the equatorial radius in pixels and SEL is the sub-Earth latitude angle.

3. Results

The 13 October 2014 intensity profile is presented in Figure 2a (red) along with the measured velocity v_{ORF} (blue) and the planetary rotation v_r (dashed black line). We have measured a gradual reduction in signal at the planet's limbs, a direct effect of the telluric seeing on the night of observations (seen in Melin et al., 2019; Thomas et al., 2023). To determine where the limbs of the planet were, we compared the emission line's spatial extent against horizontal cuts of the imager (SCAM). By scaling and then comparing the emission profile to the imager profile, we could adjust the emission line to locate the edges of the planet's disk. The integration time of the data

19448007, 2025, 7, Downloaded from https://agupubs.onlinelibrary.wiley.com/doi/10.1029/2024GL112001 by James O'Donoghue - Test , Wiley Online Library on [02/04/2025]. See the Terms and Conditions (https://onlinelibrary.wiley.com/terms-and-conditions) on Wiley Online Library for rules of use; OA articles are governed by the applicable Creative Commons License

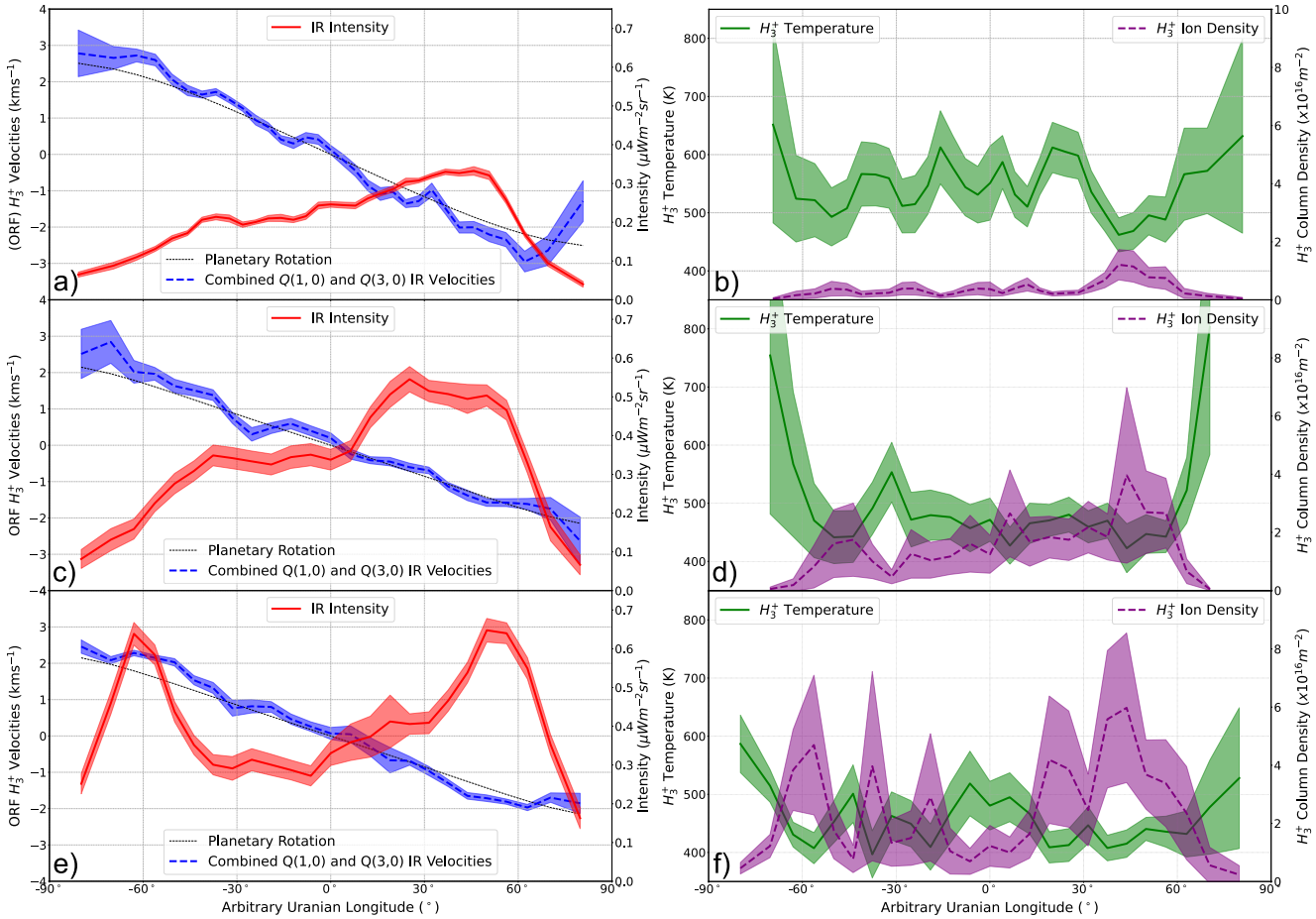

Figure 2. (a) Intensity profile of averaged Q(1, 0$^-$) and Q(3, 0$^-$) emissions observed by Keck II NIRSPEC on 13th October 2014 shown alongside the measured H_3^+ ion winds in the ORF (Observer's Reference Frame) (blue with the uncertainties shaded) compared against an arbitrary longitude. (b) Observed H_3^+ temperatures (green with uncertainties shaded) and H_3^+ column densities (purple with uncertainties shaded) for the 13th October 2014. (c) Intensity profile of averaged Q(1, 0$^-$) and Q(3, 0$^-$) emissions observed by IRTF iSHELL on 11th October 2016 at 09:00 UTC in the South position and (e) at 12:00 UTC in the same South position (red with uncertainties shaded), shown alongside the with the measured H_3^+ ion winds in the ORF (blue with the uncertainties shaded). (d) Observed H_3^+ temperatures (green with uncertainties shaded) and H_3^+ column densities (purple with uncertainties shaded) at 09:00 UTC on the 11th October 2016 and (f) at 12:00 UTC. An arbitrary Uranian longitude has been used across all plots, as the longitude is unknown for most of these observations. The same arbitrary longitude is used across plots in rows but not across columns. All uncertainties shown are equal to one standard deviation.

(~1 hr) and the high atmospheric seeing in 2014 result in an average uncertainty of ±20° longitude and ±9° latitude.

We observe a dusk enhanced emission profile in Figure 2a, which peaks at a maximum of ~0.4 μWm^{-2}sr^{-1} post noon (between 0° and 90° longitude). This profile has been observed by Melin et al., 2019 who found the average intensity profile peaked between 12 and 15 in local time (LT) or 0°–45° longitude.

We observe significant super-rotations between −90° and −46° longitude and 46°–90° longitude, up to 1.0 ± 0.6 kms^{-1} faster than planetary rotation. These super rotation features are shortly followed by a sub-rotation feature at the limb, which suggests potentially poor Gaussian fits in these regions due to the weaker SNR (shown in Supplementary Figure S1 in Supporting Information S1). Hence, we focus on super rotation features away from the limbs. Three such features are observed between, −46° to −30° between −7° and 0° and between 4° and 28° longitudes with an average 10% faster rotation than the planetary rotation. The first two ion velocity features align closely with small variability in the H_3^+ profile in Figure 2a, whereas the latter has no similar intensity feature. Across Uranus's disk, we find the ion velocities have a 14%–20% increase from planetary rotation for 2014.

In Figure 2b, we present the ionospheric temperatures (green line), alongside the calculated H_3^+ ion column density (purple dashed line) of Figure 2a. The temperatures are significant elevated at the limbs, which coincides

19448007, 2025, 7, Downloaded from https://agupubs.onlinelibrary.wiley.com/doi/10.1029/2024GL112001 by James O'Donoghue - Test , Wiley Online Library on [02/04/2025]. See the Terms and Conditions (https://onlinelibrary.wiley.com/terms-and-conditions) on Wiley Online Library for rules of use; OA articles are governed by the applicable Creative Commons License

19448007, 2025, 7, Downloaded from https://agupubs.onlinelibrary.wiley.com/doi/10.1029/2024GL112001 by James O'Donoghue - Test , Wiley Online Library on [02/04/2025]. See the Terms and Conditions (https://onlinelibrary.wiley.com/terms-and-conditions) on Wiley Online Library for rules of use; OA articles are governed by the applicable Creative Commons License

with the reduced intensities and significant super and sub-rotation velocities, both caused by lower signal and weaker SNR. Outside this region we find an average temperature of 549 ± 42K with no significant variation. Ion densities peak around ∼45° longitude and line up with the intensity peak seen in Figure 2a, suggesting this is what drives the intensity enhancement. This result also aligns with column density models of H_3^+ presented by Moore et al. (2019) when considering the solar extreme ultraviolet (EUV) radiation across the disk of Uranus, where the ion has a lifetime between 1 and 3 hr.

In Figures 2c–2f, we present measurements of intensity, ion winds, temperature and column density, on the 11 October 2016 (the remaining observations are shown in Supplementary Figures S2–S4 in Supporting Information S1). In Figures 2c and 2e, only 4 sets from the 11 are presented as these are positioned on the southern half of the planet (S as shown in Figure 1b), each figure contains data integrated over 30 min Melin et al. (2019) detected a dawn intensity enhancement (seen in Figure 1f) that was suggested to be the southern aurora, hence we have divided these 4 data sets into 2 groups; Group 1 averaged data from 08:44 and 09:14 UTC; and Group 2 averaged data from 11:42 and 12:11 UTC. We note that, due to the ∼1 hr integration and 0.67" atmospheric seeing on the night, there is a ±11° longitude blur in both sets of data.

In Figures 2c and 2e, we present the intensity profiles for Groups 1 and 2 respectively. In Figure 2e, we also observe the dawn enhancement first presented by Melin et al., 2019. At this location a 220 ± 118% increase (compared to Figure 2c) is measured, strongly suggesting a localized emission feature.

In Figures 2d and 2f, we present calculated ionospheric temperature (green line) alongside the H_3^+ column density (purple dashed line). Similar to Figure 2b we also observe high temperatures at the planet's limbs, due to the weaker SNR. For Figure 2d an average temperature of 466 ± 29 K is found whereas Figure 2f has an average temperature of 446 ± 35 K. These temperatures are 10%–20% lower than in 2014 and align with the observed long-term cooling in Uranus's upper atmosphere (Melin et al., 2011, 2019). We also observe dusk ion density enhancements in Figures 2d and 2f, with the peak around 45° longitude. We observe significant column densities in both Figures 2d and 2f with an average of $1.75 \pm 0.78 \times 10^{16}$ m^{-2} and $2.72 \pm 1.63 \times 10^{16}$ m^{-2}, which are 5–8 times larger than the average column density in 2014. We also identify enhanced column densities at the dawn event in Figure 2f, which are 3 times higher ($2.51 \pm 1.48 \times 10^{16}$ m^{-2}) than at the same longitude in Figure 2d ($8.42 \pm 6.13 \times 10^{15}$ m^{-2}). This feature combined with a lack of thermal changes strongly suggests we have observed the aurora generating localized ionization.

Focusing on the ion winds in Figures 2c and 2e, we find an average 18 ± 8% increase from planetary rotation in Figure 2c compared to an average 7 ± 4% increase in Figure 2e. For Figure 2c, we observe a localized region of sub-rotation (416 ± 186 ms^{-1} below the planetary rotation) at 26° longitude, where the remaining ion winds are either co-rotating or super rotating. For Figure 2e, we do not find this feature. Instead, two distinct regions of super-rotation are observed between −38° and −62° longitude (at 430 ± 106 ms^{-1} above planetary rotation) and 38°–62° longitude (at 256 ± 87 ms^{-1} above planetary rotation), where the dawn feature coincides with the region of dawn enhanced emissions in Figure 2e. The averaged ion flows of Figure 2c are similar to the ion flows observed in Figure 2a, whilst the same flows of Figure 2e are on average only half as super rotated compared to Figures 2a and 2c, despite higher ion flows at localized regions. This result suggests that super-rotation across Uranus is a constant feature which can vary over short-term periods (approx. 3 hrs). The exact reason for this variation is unknown, though the presence of localized emission enhancements and overall increased intensity in 2016 could be a contributing factor.

In Figure 3 we present the intensity projections of all observations between 07:00–12:00 UTC on the 11 October 2016. To mitigate the effect of smearing, we have separated the observations into the smallest coadded sets each with an integration of 30 min. We note that due to the strong dusk enhancement observed in all E-W profiles of H_3^+ emissions, we have subtracted the average intensity profile for each slit location shown in Figure 1 (North, Equator and South), so we can identify any unusual enhanced features. We identify two locations of enhanced intensities between 60°–110° longitude and 15°S–45°S as well as 190°–240° longitude and 15°S–50°S. At these peaks we observe intensity increases of ∼40%–320% suggesting high variability over this night. We previously confirmed this second enhancement to be auroral in nature and so attempted to best fit these strong emissions in latitude with Q_3^{mp} model of Uranus' aurorae (Herbert, 2009). Due to the ±11° longitude uncertainty, it is difficult to precisely determine the exact emission location with regards to the Q_3^{mp} model. We therefore completed a rough fitting of the IR emissions to sit at or close to southern aurora L shells of 3, 5, 10, and 20, due to their southern location and prior UV emissions in these L shells (Lamy et al., 2012, 2017).

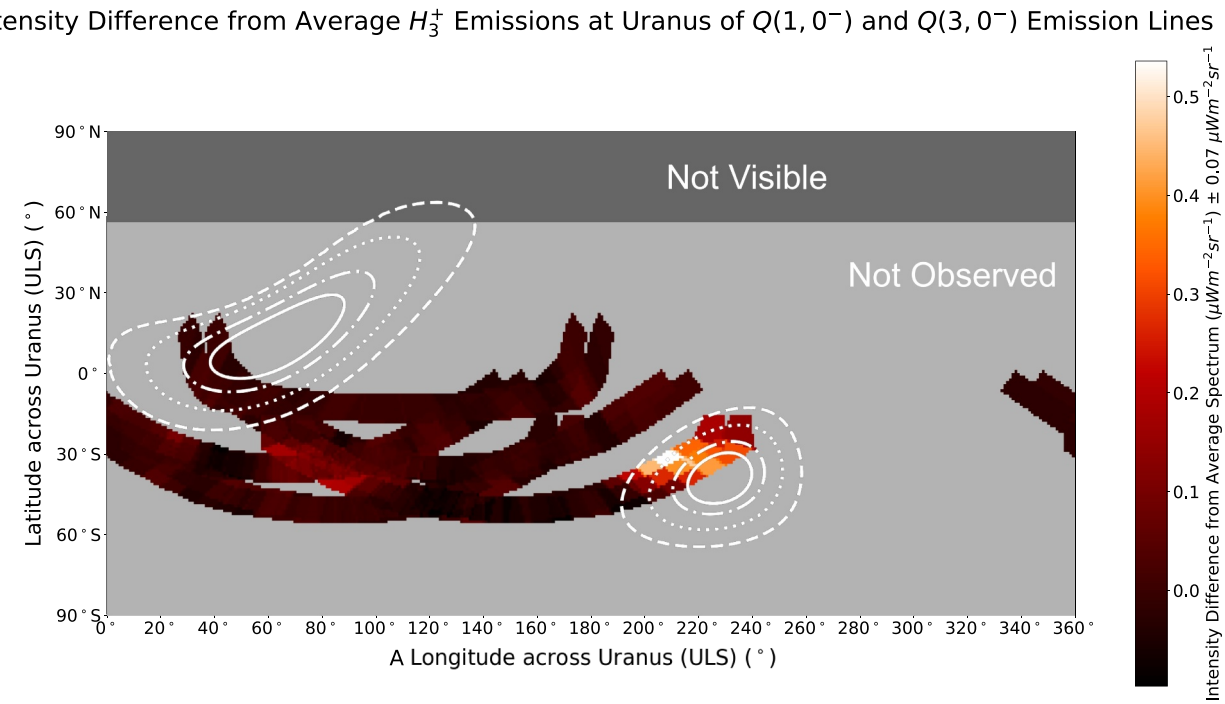

Figure 3. Planetographic mapping of the averaged Q(1, 0⁻) and Q(3, 0⁻) intensity difference (from the average emission profile at each location) mapped against the ULS longitude and latitude. White lines indicate the southern and northern model auroral ovals from the Q_3^{mp} model, where each line represents an L shell from 3 (dashed), 5 (dotted), 10 (dashed and dotted), 20 (solid).

4. Discussion

Dusk-enhanced profiles are observed across Figures 2a, 2c and 2e, but the peak intensity value differs between 2014 and 2016. In Figures 2c and 2e, between the central meridian and the dusk limb, a 55%–68% increase in the dusk enhancement is observed between 2016 and 2014. This could be explained by CIR (Corotating Interaction Region) or CME (Coronal Mass Ejection) activity in 2016. To identify solar wind conditions at Uranus at this time, models such as the 1D MHD Tao+ (Tao et al., 2005) and HUXt models (Owens et al., 2020) or the 2D MHD model of MSWIM2D (Keebler et al., 2022) can be used which observe solar wind parameters at Earth and propagated out to Uranus. With these predictions we estimate that a dynamic pressure front hit Uranus on 10 October 2016 with ±7 days of uncertainty, which falls in line with the 27 days cycle of CIR as a similar pressure front hit Uranus on the 21 September 2016. A compression on a magnetic system such as Uranus has been documented via CMEs in the UV by Lamy et al. (2012, 2017), Lamy (2020) For both Jupiter and Saturn, the RAM pressure of solar wind compressions have been observed to create variation in the planet's auroral velocity structures (Stallard et al., 2001, 2012). Hence we may expect similar variations between the 2014 and 2016 observations at Uranus. Furthermore, a compression of the magnetopause from 17 R_U to 28 R_U was observed in 1986 during the Voyager 2 flyby which occurred during a dramatic solar wind dynamic pressure enhancement (Jasinski et al., 2024). We therefore suggest that the dramatic difference between 2014 and 2016 maybe due to a CIR impacting Uranus.

As identified by Melin et al., 2019, the enhanced intensity event observed at 11:27 UTC was observed at a latitude of −45° ± 15°, with an approximate longitude of 190–240 ± 30° ULS consistent with the southern auroral region confirmed by the significant localized increases in column densities in Figure 2f. This coupled with the constant temperature (approx. 456 ± 63 K) in this location strengthens our conclusion of southern auroral activity that align with prior UV emissions (Herbert, 2009). We thus conclude that the observations on 11 October 2016 revealed a portion of the southern aurora and suggest that Uranus's aurora is not a significant source of heating in Uranus's ionosphere (Yelle & Miller, 2004).

On 13 October 2014, Keck NIRSPEC observations showed on average super rotation of 14–20 ± 15%. Three super-rotation features are observed between, −46° to −30°, −7°–0° and 4°–28° longitudes, with the first two

19448007, 2025, 7, Downloaded from https://agupubs.onlinelibrary.wiley.com/doi/10.1029/2024GL112001 by James O'Donoghue - Test , Wiley Online Library on [02/04/2025]. See the Terms and Conditions (https://onlinelibrary.wiley.com/terms-and-conditions) on Wiley Online Library for rules of use; OA articles are governed by the applicable Creative Commons License

features aligning closely with small perturbations in the H_3^+ intensity; however, they are not significant enough to suggest they may be related. We also observe no significant variability in the temperature (4% which can be explained by the 10% calculated uncertainty) or column density (24% which is covered by the 45% calculated uncertainty) in these regions. Therefore, the reason for these localized super-rotation values is unknown. The 11 October 2016 IRTF iSHELL observations also showed an average super-rotation between 7 ± 4% to 18 ± 8%. Away from the limbs toward the center of the planet, we observe two distinct locations of super-rotation (>200 ms^{-1}) and one location of sub-rotation at 09:00 UTC, which disappear or move by 12:00 UTC. Our suggestion is that the southern aurora could explain the velocity changes in these regions.

Although stratospheric winds have been measured at Jupiter and Saturn (Flasar et al., 2004, 2005) no such measurements have been taken at Uranus. We instead focus on the tropospheric winds (found below the stratosphere). Tropospheric wind speeds have been investigated by Hammel et al. (2001), Sromovsky and Fry (2005), Hueso and Sánchez-Lavega (2019) and Soyuer et al. (2020) identifying wind speed variation depending on latitude. If we assume the zonal winds at the troposphere continue out to the ionosphere this could explain the super-rotation events. For the 2014 data, we expect coverage between 3°N–24°S latitudinal range and between latitudes of 22°N–18°S, 0°S–40°S and 16°S–55°S for the 2016 data. Hence for 2014, we would expect a maximum sub-rotation between 100 and 0 ms^{-1} for 2014 and a maximum super-rotation of ∼150 ms^{-1} to a maximum sub rotation of 100 ms^{-1} for 2016 (Hammel et al., 2001) which is too small to explain the velocity shears observed. Therefore, the super-rotation in Uranus's ionosphere cannot be explained by the tropospheric winds.

This outcome is unsurprising given that Johnson et al. (2017) found the equatorial ionosphere of Jupiter to corotate with the planet's rotation, whilst tropospheric winds varied across the same latitudes. Though equatorial ion winds have not been observed remotely at Saturn, the tropospheric winds have been well documented by Cassini (Barbara & Del Genio, 2021; Sánchez-Lavega et al., 2011). These investigations did find that toward the equator, the tropospheric winds could super-rotate from 150 ms^{-1} up to 400 ms^{-1} and on average decrease close toward corotation at the limbs, the opposite of what has been observed at Uranus. From this comparison, we conclude that there is an average super-rotation observed across multiple equatorial and southern latitudes which may be disconnected from the tropospheric zonal wind system.

5. Conclusion

We have successfully extracted H_3^+ ion velocities from both Keck II NIRSPEC and IRTF iSHELL data for the first time. We observe an average super rotation of 18 ± 15% in 2014 and between 7 ± 4% to 18 ± 8% in 2016 above the planetary rotation. Close to the southern aurora we observe a localized region of super-rotation (13% of planetary rotation increase). Further investigations should aim to observe ion velocities of the aurora away from the limb if possible. We demonstrate that the enhanced intensity feature observed on the dawn reported by Melin et al., 2019, is driven by significantly enhanced column densities (peaking at 2.51×10^{16} m^{-2}) and minimal temperature changes, proving this feature to be a section of the NIR southern aurora. We suggest that the average enhancement observed in 2016 was due to an increase in auroral precipitation associated with a CMI impact predicted to hit Uranus around the time of observation.

Data Availability Statement

The data presented herein were obtained at the W. M. Keck Observatory, which is operated as a scientific partnership among the California Institute of Technology, the University of California and the National Aeronautics and Space Administration. The Observatory was made possible by the generous financial support of the W. M. Keck Foundation. The authors wish to recognize and acknowledge the very significant cultural role and reverence that the summit of Maunakea has always had within the indigenous Hawaiian community. We are most fortunate to have the opportunity to conduct observations from this mountain. N.D.R, R.J.V., H.K., T.S.S. and H.M. were Visiting Astronomers at the Infrared Telescope Facility, which is operated by the University of Hawai'i under contract 80HQTR19D0030 with the National Aeronautics and Space Administration. The raw data from NIRSPEC used in this study are publicly available on the Keck Observatory Archive (KOA) at https://koa.ipac.caltech.edu/cgi-bin/bgServices/nph-bgExec?bgApp=/KOA/nph-KOA&instrument_ns=nirspec&daterange=20141012&filetype=both, no registration is required. Raw data from iSHELL used in this study are publicly

19448007, 2025, 7, Downloaded from https://agupubs.onlinelibrary.wiley.com/doi/10.1029/2024GL112001 by James O'Donoghue - Test , Wiley Online Library on [02/04/2025]. See the Terms and Conditions (https://onlinelibrary.wiley.com/terms-and-conditions) on Wiley Online Library for rules of use; OA articles are governed by the applicable Creative Commons License

available on the NASA/IPAC Infrared Science Archive at https://irsa.ipac.caltech.edu/applications/irtf/, no registration is required. Reduced and calibrated images used in this current study can be obtained through the RedSpec code (discussed below) with the final data used in the Figures of this manuscript available on GitHub with the Source Data and data repository link in Thomas, 2024, no registration is required. RedSpec is a data reduction package in IDL, designed to reduce and process spectral images from NIRSPEC and is available at https://www2.keck.hawaii.edu/inst/nirspec/redspec. No registration is required. IRTF spectral images from iSHELL were similarly reduced with Spextool and is available at https://irtfweb.ifa.hawaii.edu/research/dr_resources/. Version 0.5.2 of h3ppy is an H_3^+ emission modeling and fitting package in Python and is preserved at https://github.com/henrikmelin/h3ppy, no registration is required. All remaining code used to extract from the reduced data to the final figures can be found in the following data repository link in Thomas (2024), no registration is required.

Acknowledgments
The UK STFC studentships ST/T506242/1 and ST/N504117/1 supported the work of EMT and MNC respectively. The STFC James Webb Fellowship (ST/W001527/1) at the University of Leicester, UK supported HM, and the UK STFC Consolidated Grant ST/N000749/1 supported TSS. The NERC EISCAT 3D grant NE/W002914/1 supported the work of REJ. The STFC Ernest Rutherford Fellowship ST/X003426/1 supported the work of JO.

References

Barbara, J. M., & Del Genio, A. D. (2021). Tropopause and lower stratosphere winds and eddy fluxes on Saturn as seen by Cassini imaging. *Icarus*, *354*, 114095. https://doi.org/10.1016/j.icarus.2020.114095

Cao, X., & Paty, C. (2017). Diurnal and seasonal variability of Uranus's magnetosphere. *Journal of Geophysical Research: Space Physics*, *122*(6), 6318–6331. https://doi.org/10.1002/2017ja024063

Cao, X., & Paty, C. (2021). Asymmetric structure of Uranus' magnetopause controlled by IMF and planetary rotation. *Geophysical Research Letters*, *48*(4), e2020GL091273. https://doi.org/10.1029/2020gl091273

Chowdhury, M. N., Stallard, T. S., Baines, K. H., Provan, G., Melin, H., Hunt, G. J., et al. (2022). Saturn's weather-driven aurorae modulate oscillations in the magnetic field and radio emissions. *Geophysical Research Letters*, *49*(3), e2021GL096492. https://doi.org/10.1029/2021GL096492

Chowdhury, M. N., Stallard, T. S., Melin, H., & Johnson, R. E. (2019). Exploring key characteristics in Saturn's infrared auroral emissions using VLT-CRIRES: Intensities, ion line-of-sight velocities, and rotational temperatures. *Geophysical Research Letters*, *46*(13), 7137–7146. https://doi.org/10.1029/2019gl083250

Emerich, C., Jaffel, L. B., Clarke, J. T., Prange, R., Gladstone, G. R., Sommeria, J., & Ballester, G. (1996). Evidence for supersonic turbulence in the upper atmosphere of Jupiter. *Science*, *273*(5278), 1085–1087. https://doi.org/10.1126/science.273.5278.1085

Flasar, F. M., Achterberg, R. K., Conrath, B. J., Pearl, J. C., Bjoraker, G. L., Jennings, D. E., et al. (2005). Temperatures, winds, and composition in the Saturnian system. *Science*, *307*(5713), 1247–1251. https://doi.org/10.1126/science.1105806

Flasar, F. M., Kunde, V. G., Achterberg, R. K., Conrath, B. J., Simon-Miller, A. A., Nixon, C. A., et al. (2004). An intense stratospheric jet on Jupiter. *Nature*, *427*(6970), 132–135. https://doi.org/10.1038/nature02142

Hammel, H. B., Rages, K., Lockwood, G. W., Karkoschka, E., & de Pater, I. (2001). New measurements of the winds of Uranus. *Icarus*, *153*(2), 229–235. https://doi.org/10.1006/icar.2001.6689

Herbert, F. (2009). Aurora and magnetic field of Uranus. *Journal of Geophysical Research*, *114*(A11), A11206. https://doi.org/10.1029/2009JA014394

Herbert, F., & Sandel, B. R. (1994). The Uranian aurora and its relationship to the magnetosphere. *Journal of Geophysical Research*, *99*(A3), 4143–4160. https://doi.org/10.1029/93ja02673

Hueso, R., & Sánchez-Lavega, A. (2019). Atmospheric dynamics and vertical structure of Uranus and Neptune's weather layers. *Space Science Reviews*, *215*(8), 52. https://doi.org/10.1007/s11214-019-0618-6

Jasinski, J. M., Cochrane, C. J., Jia, X., Dunn, W. R., Roussos, E., Nordheim, T. A., et al. (2024). The anomalous state of Uranus's magnetosphere during the Voyager 2 flyby. *Nature Astronomy*, *9*(1), 66–74. https://doi.org/10.1038/s41550-024-02389-3

Johnson, R. E., Melin, H., Stallard, T. S., Tao, C., Nichols, J. D., & Chowdhury, M. N. (2018). Mapping H_3^+ temperatures in Jupiter's northern auroral ionosphere using VLT-CRIRES. *Journal of Geophysical Research: Space Physics*, *123*(7), 5990–6008. https://doi.org/10.1029/2018ja025511

Johnson, R. E., Stallard, T. S., Melin, H., Nichols, J. D., & Cowley, S. W. H. (2017). Jupiter's polar ionospheric flows: High resolution mapping of spectral intensity and line-of-sight velocity of H_3^+ ions. *Journal of Geophysics Research: Space Physics*, *122*(7), 7599–7618. https://doi.org/10.1002/2017JA024176

Keebler, T. B., Tóth, G., Zieger, B., & Opher, M. (2022). MSWIM2D: Two-dimensional outer heliosphere solar wind modeling. *The Astrophysical Journal - Supplement Series*, *260*(2), 43. https://doi.org/10.3847/1538-4365/ac67eb

Khurana, K. K., Dougherty, M. K., Provan, G., Hunt, G. J., Kivelson, M. G., Cowley, S. W. H., et al. (2018). Discovery of atmospheric-wind-driven electric currents in Saturn's magnetosphere in the gap between Saturn and its rings. *Geophysical Research Letters*, *45*(19), 10–068. https://doi.org/10.1029/2018gl078256

Lamy, L. (2020). Auroral emissions from Uranus and Neptune. *Philosophical Transactions of the Royal Society A*, *378*(2187), 20190481. https://doi.org/10.1098/rsta.2019.0481

Lamy, L., Berland, C., Andre, N., Prange, R., Fouchet, T., Encrenaz, T., et al. (2018). Analysis of HST, VLT and gemini coordinated observations of Uranus Late 2017: A multi-spectral search for auroral signatures. *Société Francaise d'Astronomie et d'Astrophysique (SF2A)*. https://doi.org/10.48550/arXiv.1810.08526

Lamy, L., Prangé, R., Hansen, K. C., Clarke, J. T., Zarka, P., Cecconi, B., et al. (2012). Earth-based detection of Uranus' aurorae. *Geophysical Research Letters*, *39*(7). https://doi.org/10.1029/2012GL051312

Lamy, L., Prangé, R., Hansen, K. C., Tao, C., Cowley, S. W. H., Stallard, T. S., et al. (2017). The aurorae of Uranus past equinox. *Journal of Geophysical Research: Space Physics*, *122*(4), 3997–4008. https://doi.org/10.1002/2017JA023918

McLean, I. S., Becklin, E. E., Bendiksen, O., Brims, G., Canfield, J., Figer, D. F., et al. (1998). The design and development of NIRSPEC: A near-infrared echelle spectrograph for the Keck II telescope. *Proceedings of SPIE*, *3354*, 566.

Melin, H., Fletcher, L. N., Stallard, T. S., Miller, S., Trafton, L. M., Moore, L., et al. (2019). The H_3^+ ionosphere of Uranus: Decades-long cooling and local-time morphology. *Philosophical Transactions of the Royal Society A*, *377*(2154), 20180408. https://doi.org/10.1098/rsta.2018.0408

Melin, H., Stallard, T., Miller, S., Trafton, L. M., Encrenaz, T., & Geballe, T. R. (2011). Seasonal variability in the ionosphere of Uranus. *The Astrophysical Journal*, *729*(2), 134. https://doi.org/10.1088/0004-637x/729/2/134

19448007, 2025, 7, Downloaded from https://agupubs.onlinelibrary.wiley.com/doi/10.1029/2024GL112001 by James O'Donoghue - Test , Wiley Online Library on [02/04/2025]. See the Terms and Conditions (https://onlinelibrary.wiley.com/terms-and-conditions) on Wiley Online Library for rules of use; OA articles are governed by the applicable Creative Commons License

Miller, S., Tennyson, J., Geballe, T. R., & Stallard, T. (2020). Thirty years of H 3+ astronomy. *Reviews of Modern Physics*, *92*(3), 035003. https://doi.org/10.1103/revmodphys.92.035003

Moore, L., Melin, H., O'Donoghue, J., Stallard, T. S., Moses, J. I., Galand, M., et al. (2019). Modelling H_3^+ in planetary atmospheres: Effects of vertical gradients on observed quantities. *Philosophical Transactions of the Royal Society A: Mathematical, Physical and Engineering Sciences*, *377*(2154), 20190067. https://doi.org/10.1098/rsta.2019.0067

Moore, L., Moses, J. I., Melin, H., Stallard, T. S., & O'Donoghue, J. (2020). Atmospheric implications of the lack of H_3+ detection at Neptune. *Philosophical Transactions of the Royal Astronomical Society A*, *378*(2187), 20200100. https://doi.org/10.1098/rsta.2020.0100

Ness, N. F., Acuña, M. H., Behannon, K. W., Burlaga, L. F., Connerney, J. E., Lepping, R. P., & Neubauer, F. M. (1986). Magnetic fields at Uranus. *Science*, *233*(4759), 85–89. https://doi.org/10.1126/science.233.4759.85

O'Donoghue, J., Moore, L., Connerney, J., Melin, H., Stallard, T. S., Miller, S., & Baines, K. H. (2019). Observations of the chemical and thermal response of "ring rain"on Saturn's ionosphere. *Icarus*, *322*, 251–260. https://doi.org/10.1016/j.icarus.2018.10.027

Owens, M., Lang, M., Barnard, L., Riley, P., Ben-Nun, M., Scott, C. J., et al. (2020). A computationally efficient, time-dependent model of the solar wind for use as a surrogate to three-dimensional numerical magnetohydrodynamic simulations. *Solar Physics*, *295*(3), 43. https://doi.org/10.1007/s11207-020-01605-3

Rayner, J., Bond, T., Bonnet, M., Jaffe, D., Muller, G., & Tokunaga, A. (2012). iSHELL: A 1-5 micron cross-dispersed R=70,000 immersion grating spectrograph for IRTF. In *Ground-based and airborne instrumentation for astronomy IV*. SPIE. https://doi.org/10.1117/12.925511

Sánchez-Lavega, A., Río-Gaztelurrutia, T. D., Hueso, R., Gómez-Forrellad, J. M., Sanz-Requena, J. F., Legarreta, J., et al. (2011). Deep winds beneath Saturn's upper clouds from a seasonal long-lived planetary-scale storm. *Nature*, *475*(7354), 71–74. https://doi.org/10.1038/nature10203

Soyuer, D., Soubiran, F., & Helled, R. (2020). Constraining the depth of the winds on Uranus and Neptune via Ohmic dissipation. *Monthly Notices of the Royal Astronomical Society*, *498*(1), 621–638. https://doi.org/10.1093/mnras/staa2461

Sromovsky, L. A., & Fry, P. M. (2005). Dynamics of cloud features on Uranus. *Icarus*, *179*(2), 459–484. https://doi.org/10.1016/j.icarus.2005.07.022

Stallard, T., Miller, S., Millward, G., & Joseph, R. D. (2001). On the dynamics of the Jovian ionosphere and thermosphere: I. The measurement of ion winds. *Icarus*, *154*(2), 475–491. https://doi.org/10.1006/icar.2001.6681

Stallard, T. S., Baines, K. H., Melin, H., Bradley, T. J., Moore, L., O'Donoghue, J., et al. (2019). Local-time averaged maps of H3+ emission, temperature and ion winds. *Philosophical Transactions of the Royal Society A*, *377*(2154), 20180405. https://doi.org/10.1098/rsta.2018.0405

Stallard, T. S., Masters, A., Miller, S., Melin, H., Bunce, E. J., Arridge, C. S., et al. (2012). Saturn's auroral/polar H3+ infrared emission: The effect of solar wind compression. *Journal of Geophysical Research*, *117*(A12), A12302. https://doi.org/10.1029/2012ja018201

Stallard, T. S., Miller, S., Lystrup, M., Achilleos, N., Arridge, C., & Dougherty, M. (2008). Dusk-brightening event in Saturn's H3+ Aurora. *The Astrophysical Journal*, *673*(2), L203–L206. https://doi.org/10.1086/527545

Stallard, T. S., Miller, S., Melin, H., Lystrup, M., Dougherty, M., & Achilleos, N. (2007a). Saturn's auroral polar H3+ infrared emission. I. General morphology and ion velocity structure. *Icarus*, *189*, 1–13. https://doi.org/10.1016/j.icarus.2006.12.027

Stallard, T. S., Miller, S., Trafton, L. M., Geballe, T. R., & Joseph, R. D. (2004). Ion winds in Saturn's southern auroral/polar region. *Icarus*, *167*(1), 204–211. https://doi.org/10.1016/j.icarus.2003.09.006

Stallard, T. S., Smith, C., Miller, S., Melin, H., Lystrup, M., Aylward, A., et al. (2007b). Saturn's auroral polar H3+ infrared emission. II. A comparison with plasma flow models. *Icarus*, *191*(2), 678–690. https://doi.org/10.1016/j.icarus.2007.05.016

Tao, C., Kataoka, R., Fukunishi, H., Takahashi, Y., & Yokoyama, T. (2005). Magnetic field variations in the Jovian magnetotail induced by solar wind dynamic pressure enhancements. *Journal of Geophysical Research*, *110*(A11), A11208. https://doi.org/10.1029/2004ja010959

Thomas, E. M. (2024). IRTFKECK_H3_Vels repository v0.1.0-alpha [Collection]. *Zenodo*, *488*. https://doi.org/10.5281/zenodo.14162429

Thomas, E. M., Melin, H., Stallard, T. S., Chowdhury, M. N., Wang, R., Knowles, K., & Miller, S. (2023). Detection of the infrared aurora at Uranus with Keck-NIRSPEC. *Nature Astronomy*, *7*(12), 1–8. https://doi.org/10.1038/s41550-023-02096-5

Tóth, G., Kovács, D., Hansen, K. C., & Gombosi, T. I. (2004). Three-dimensional MHD simulations of the magnetosphere of Uranus. *Journal of Geophysical Research*, *109*(A11), A11210. https://doi.org/10.1029/2004JA010406

Vasyliunas, V. M. (1986). The convection-dominated magnetosphere of Uranus. *Geophysical Research Letters*, *13*(7), 621–623. https://doi.org/10.1029/gl013i007p00621

Wang, R., Stallard, T. S., Melin, H., Baines, K. H., Achilleos, N., Rymer, A. M., et al. (2023). Asymmetric ionospheric jets in Jupiter's aurora. *Journal of Geophysical Research: Space Physics*, *128*(12), e2023JA031861. https://doi.org/10.1029/2023ja031861

Yelle, R. V., & Miller, S. (2004). Jupiter's thermosphere and ionosphere. *Jupiter: The planet, satellites and magnetosphere*, *1*, 185–218.

19448007, 2025, 7, Downloaded from https://agupubs.onlinelibrary.wiley.com/doi/10.1029/2024GL112001 by James O'Donoghue - Test , Wiley Online Library on [02/04/2025]. See the Terms and Conditions (https://onlinelibrary.wiley.com/terms-and-conditions) on Wiley Online Library for rules of use; OA articles are governed by the applicable Creative Commons License